Microb Ecol (2017) 73:815–826
DOI 10.1007/s00248-016-0913-7

ENVIRONMENTAL MICROBIOLOGY

Microbial Life and Death in a Foxing Stain: a Suggested Mechanism of Photographic Prints Defacement

Maria Carla Sclocchi[1] · Lucia Kraková[2] · Flavia Pinzari[3,4] · Piero Colaizzi[1] · Marina Bicchieri[1] · Nikoleta Šaková[2] · Domenico Pangallo[2]

Received: 5 August 2016 / Accepted: 5 December 2016 / Published online: 15 December 2016

Abstract The gelatin-silver halide black and white prints represent an enormous photography heritage with a great value. Unaesthetic phenomena, the foxing stains that are caused by microbial growth on surface, have been described in stamps, drawings, books, and tissues but, until now, scarcely for photographic materials. In this study, a combination of various techniques, including culture-dependent and culture-independent approaches (RNA and DNA analysis), scanning electron microscopy-energy dispersive spectroscopy (SEM-EDS) and μ-Raman spectroscopy supported by X-ray fluorescence analysis (XRF), permitted to describe the microbial contamination dynamics of foxing stains present on the surface of two gelatin-silver halide photographs. The investigation provided also information on the effects of microbial activity on the materials' chemistry of the two prints. The action of microbial community resulted locally in either (a) formation of mixed aluminum-iron-potassium phosphate compounds that could be attributed to the hydrolytic activity of bacteria, (b) leaching of barite, (c) precipitation of a mixture of oxides, and (d) a change in the barium sulfate chemical structures.

Keywords Foxing · Gelatin-silver print · Molds · Nucleic acids analysis · SEM · μ-Raman

Introduction

In the last 10 years, scientific studies on photographic and cinematographic heritage preserved in archives and libraries have increased because of the vulnerability shown by these materials and the damage caused by improper storage settings [8, 10, 21, 28]. All photographic and cinematographic items are multilayered materials composed of organic compounds and inorganic elements, where microorganisms can be active under favorable conditions.

The gelatin-silver halide black and white prints, produced mainly in the twentieth century, represent an enormous photography heritage with a great value, being a part of archival documents, family albums, and also of artistic, archeological, and historical collections. A gelatin print is generally constituted by (i) a layer of gelatine, where the image is created, with emulsified silver salt (a photosensitive substance finely dispersed in gelatine) and (ii) a primary paper support covered with a layer of barium sulfate (baryta) that makes the paper as smooth as possible and suitable for receiving the emulsion. The photographic printing paper is usually of high quality, highly refined, free of lignin, and produced with particular expedients. Photographic prints, especially the artistic ones, were usually mounted on a secondary support, to protect them at usage and handling, and were stored in boxes. These preventive measures, however, did not always assure their long-term preservation. The use of cartons and glues of

Electronic supplementary material The online version of this article (doi:10.1007/s00248-016-0913-7) contains supplementary material, which is available to authorized users.

✉ Domenico Pangallo
domenico.pangallo@savba.sk

[1] Istituto Centrale Restauro e Conservazione Patrimonio Archivistico e Librario (ICRCPAL),MIBACT, Rome, Italy

[2] Institute of Molecular Biology, Slovak Academy of Sciences, Bratislava, Slovakia

[3] Consiglio per la ricerca in agricoltura e l'analisi dell'economia agraria, Centro di ricerca per lo studio delle Relazioni tra Pianta e Suolo (CREA-RPS), Rome, Italy

[4] Life Sciences Department, Natural History Museum, Cromwell Road, London SW7 5BD, UK

lower quality, in fact, could produce irreversible damage, and the photographs were susceptible to microbial contamination due to the presence of different organic and inorganic components [13].

Some phenomena that can deface and damage photographic materials, destroying forever their readability, are well-known for other kinds of heritage objects, like books and prints. This is the case of foxing stains that have been described in stamps, drawings, books, and tissues but, until now, scarcely for photographic materials [5, 32]. Despite the lack of published case studies, the foxing staining of photographic prints is a common phenomenon. In the last years, it has been demonstrated that two kinds of foxing exist, namely, biological and chemical can exist and are clearly detectable and can be differentiated by the topographic modification induced in the attacked support [12, 26].

The objectives of this investigations were the following: (a) to study the nature and origin of stains similar to foxing on the surface of gelatin prints; (b) to screen the microbiome developing on photographs when stored in metallic drawers of common use, which apparently favor microbial growth; and (c) to evaluate the role of a different chemical composition and manufacture of the photographs in the defacement phenomena.

In this work, the foxing-like stains appearance on two gelatine-silver prints supported by cardboard were assessed by means of classical microbiological culturing, culture-independent approach, scanning electron microscopy-energy dispersive spectroscopy (SEM-EDS), and μ-Raman spectroscopy supported by X-ray fluorescence analysis (XRF). The techniques were applied to two prints, collecting data from attacked and not attacked areas, in order to point out the possible differences, caused by the action of microorganisms.

Materials and Methods

Photographs, Sampling, Microbial Cultivation, and Identification

Two different gelatine-silver photographs (inv. 15438 and inv. 27371F from the American Academy of Rome collection) were investigated in this report. The prints were composed of different types of photographic paper and of a secondary cardboard support of different thickness, manufacturing, and quality; they showed an identical type of biological alteration.

In the initial phase of the study, a sudden and prolonged phase of alteration of temperature and humidity conditions was recorded in the photo library, located at the street level of the storage building, (T = from 22 to 18 °C; RH = 55 to 67%). The prints had been long retained within metallic drawer units and showed numerous small spots on surface associated with the development of a fungal mycelium network.

The biological samples were collected by the use of an adhesive tape (Fungi Tape™, DID Milan, Italy), with little adhesive strength that allowed to capture the microorganisms with no damage of the photograph. The samples were subsequently divided to different portions to be utilized for microbiological cultivation, SEM observation, and DNA and RNA extraction.

Adhesive tape strip subsamples were immersed in different cultivation media: Malt Extract agar (MEA) and Dichloran-Glycerol (DG18) (both from Oxoid, Basingstoke, UK) for fungi and Biolog™ Universal Growth agar (RIGEL s.r.l., Rome, Italy) for bacteria. The agar media were supplemented with either cycloheximide (50 mg l^{-1}; Sigma-Aldrich, Seelze, Germany) or chloramphenicol (50 mg l^{-1}; Sigma-Aldrich) in order to avoid the growth of fungi and bacteria, respectively. All the bacterial and fungal plates were incubated at room temperature (22–26 °C) for about 5 days–2 weeks.

DNA of fungal isolates was extracted by Ron's fungal DNA mini kit (Bioron, Ludwigshafen, Germany), according to the instructions of the manufacturer. The fungal ITS region was amplified with the primers ITS1 (5′-TCC GTA GGT GAA CCT GCG G-3′) and ITS4 (5′-TCC TCC GCT TAT TGA TAT GC-3′) [34]. The 25 μl PCR mixture contained 50 pmol of each primer, 200 μmol l^{-1} of dNTPs (Life Technologies, Gaithersburg, MD, USA), 1.5 U HotStar Taq plus DNA polymerase (Qiagen, Hilden, Germany), 1× PCR buffer, and 3 μl of the extracted DNA (the template). The PCR program consisted of an initial denaturation at 94 °C for 5 min, followed by 30 cycles (denaturation at 94 °C for 30 s, annealing at 54 °C for 45 s, extension at 72 °C for 1 min) and a final polymerization step at 72 °C for 10 min. The resulting PCR products from fungal isolates were purified using ExoSAP-IT (Affymetrix, Cleveland, OH, USA) and sequenced at a commercial facility (GATC-Biotech, Konstanz, Germany). The resulting sequences were directly compared with those in GenBank using BLAST program (http://blast.ncbi.nlm.nih.gov/Blast.cgi) and were subsequently deposited in GenBank under the accession numbers KU363957–KU363960.

Optical Microscopy and SEM-EDS Analysis

Adhesive tape samples and thin sections obtained by conservators from the edge of the prints were analyzed using a variable pressure SEM instrument (EVO50, Carl-Zeiss Electron Microscopy Group) fitted with a detector for electron backscattered diffraction (BSD). Only following an initial observation of the samples using SEM in VP mode at 20 kV, some of the samples were coated in gold (using a Baltec Sputter Coater) and then subjected to further analysis in high vacuum (HV) mode. Sputtering was performed under an argon gas flow at a working distance of 50 mm at 0.05 mbar, and

a current of 40 mA for 60 s, so as to create a film of gold of about 15 nm thickness.

Chemical characterization of the inorganic constituents of the samples was performed by means of electron dispersive spectroscopy (EDS). Reference elemental intensities acquired from pure compounds (standards) are commonly utilized for calibrating SEM-EDX systems. In the case study described in this paper, conventional ZAF correction integrated into an Oxford INCA 250 microanalysis package (Oxford Instruments) was applied to the spectrum dataset. The EDS measurements were taken at several points across the samples, where possible spotting of different components was distinguishable by SEM-BSD imaging (gelatine, baryta layer, precipitated minerals and particles, paper fibers). The data obtained were used for a series of comparisons aimed at evaluating the differences between the prints. One-way analysis of variance (ANOVA) was used when comparing the different components present in the samples and the significance of the differences was tested at 95% confidence. ANOVA was followed by a post hoc analysis using Tukey's honestly significant difference (HSD) test [31].

RAMAN and XRF Analyses

The original prints were directly analyzed in a non-destructive way both by Raman spectroscopy and by XRF, without any sampling. It was then possible to collect spectra from different areas signs of alteration were present or absent.

Raman spectroscopic measurements were performed by means of a Renishaw inVia Reflex Raman microscope equipped with a Renishaw diode laser at 785 nm and a 1200 line mm^{-1} grating to disperse the backscattered light. The Raman signal was detected by a Peltier-cooled (−70 °C) deep depletion charge-coupled device (CCD RD-VIU, 578 × 384 pixel) optimized for near-infrared and ultraviolet regions. The nominal spectral resolution obtained for the measurements was approx. 3 cm^{-1}. The system, equipped with a Leica DMLM microscope to focus the laser on the sample and a color video camera, allows for positioning of the sample and selection of a specific region for the investigation. Spectral acquisitions (1–10 accumulations, 50 s each) were performed with a 50× objective (N.A. 0.75). Under these conditions, the laser spot measured approx. 20 μm^2. Depending on the sample investigated, the laser power was reduced with neutral density filters up to 0.03 mW.

To obtain information on the elements present in the photographs also as impurities, some XRF spectra were recorded by means of an Assing Lithos 3000 portable spectrometer, equipped with a Mo X-ray tube. In this experiment, the 2-mm collimator was used together with a Zr filter. A red laser (695 nm) and a camera (both integrated into the system and controlled by the instrument software) were used to choose the area to be sampled. Measurements were performed with the tube operating at 25 kV, 0.300 mA, in the 0–25 keV range with a resolution of 160 eV at 5.9 keV, lasting 10–60 min for each acquisition.

DNA and RNA Extraction from Photographic Samples

Total DNA, directly from a portion of adhesive tape of the samples inv. 15438 and inv. 27371F, was extracted by the PowerSoil® DNA Isolation Kit (MO BIO Laboratories, Carlsbad, CA, USA), according to the protocol of the manufacturer. RNA was extracted from another portion of adhesive tape of the same samples as above using Spectrum™ Plant Total RNA Kit (Sigma-Aldrich) following the instructions of the producer (protocol B). After elution, RNA was treated by DNase I (Thermo Fisher Scientific) and directly transcripted to cDNA. The rest of RNA was stored at −80 °C. In vitro transcription of RNA was done by Invitrogen cloned AMV First-Strand cDNA Synthesis Kit (Invitrogen, Carlsbad, CA, USA) according to the protocol of the manufacturer. Obtained cDNA was used as a template for PCR amplification.

PCR Amplification of DNA/cDNA from Photograph Samples

The bacterial 16S rRNA fragment was amplified using the primers 27f (5′-AGA GTT TGA TCC TGG CTC AG-3′) and 685r (5′-TCT ACG CAT TTC ACC GCT AC-3′) [20]. PCR mixture contained 1× PCR buffer, 2.5 mmol l^{-1} $MgCl_2$, 200 μmol l^{-1} dNTPs, 30 pmol of each primer, 2 U HotStarTaq plus DNA polymerase (Qiagen), and 3 μl of template DNA/cDNA in the total reaction volume of 50 μl. The following thermocycling program was used: 5 min denaturation at 95 °C, followed by 35 cycles of a 45 s at 94 °C, 1 min at 54 °C, and 1 min at 72 °C, and final extension was run at 72 °C for 8 min.

The eukaryotic 28S rRNA gene was amplified by primers NL1 (5′-GCA TAT CAA TAA GCG GAG GAA AAG-3′) and NL4 (5′-GGT CCG TGT TTC AAG ACG G-3′) [19]. The PCR mixture was the same as described above; the PCR program was as follows: initial denaturation step at 95 °C for 5 min, 35 cycles (95 °C for 1 min, 52 °C for 1 min, 72 °C for 1 min), and a final polymerization at 72 °C for 8 min.

For each DNA/cDNA target (16S rRNA and 28S rRNA), two reactions of 50 μl (100 μl altogether) were run. Products of the two reactions of each DNA/cDNA target were pooled and 5 μl were analyzed by electrophoresis in 1.5% agarose gel and stained by ethidium bromide. The rest was purified by QIAquick PCR Purification Kit (Qiagen) and eluted in 20 μl of sterile distilled water. This purified PCR product was used in all cloning approaches and semi-nested PCR amplifications combined with DGGE fingerprinting.

Semi-nested PCR and DGGE Fingerprint Analysis

The PCR product of the first step (2 μl) was used as a template in the second amplification, a semi-nested PCR for each DNA/cDNA target. The 16S rDNA was re-amplified with primers 518f (5′-CCA GCA GCC GCG GTA AT-3′) [9] and 685r-GC (5′-CGC CCG CCG CGC GCG GCG GGC GGG GCG GGG GCA CGG GGG GTC TAC GCA TTT CAC CGC TAC-3′). The semi-nested PCR for 28S rRNA utilized the primers NL1-CG (5′-CGC CCG CCG CGC GCG GCG GGC GGG GCG GGG GCA CGG GGG GGC ATA TCA ATA AGC GGA GGA AAA G -3′) and LS2 (5′-ATT CCC AAA CAA CTC GAC TC-3′) [11]. The PCR conditions were the same as stated in the previous paragraph. Two semi-nested PCR products (2 reactions of 50 μl) for each DNA/cDNA target were pooled, checked by electrophoresis in agarose gel, precipitated with 96% ethanol, and then resuspended in 20 μl H_2O; the precipitate (10 μl) was analyzed by DGGE in 8% polyacrylamide gel (acrylamid e-bisacrylamide 37.5:1) with the denaturation gradient of 25–55% for separation of 16S rRNA amplicons, and 20–50% for separation of 28S rRNA amplicons (100% denaturant contained 7 mol l^{-1} urea and 40% (*v*/*v*) formamide). DGGE was run on DCode System (Bio-Rad) in 0.5 × TAE (20 mmol l^{-1} Tris, 10 mmol l^{-1} acetate, 0.5 mmol l^{-1} Na_2 EDTA; pH 8.0) at 200 V and 60 °C for 3 h for bacteria or for 5 h for eukaryotes.

Construction of Clone Libraries and Sequencing

The rest of the PCR products from the first amplifications were used for the construction of bacterial 16S rRNA and eukaryotic 28S rRNA clone libraries. Briefly, the PCR products were ligated to pGEM-T Easy vector (Promega, Madison, WI, USA), transformed to *Escherichia coli* XLI-Blue, and spread to LB plates with ampicillin (100 μg ml^{-1}), X-Gal (0.1 mmol l^{-1}), and IPTG (0.2 mmol l^{-1}). A number of about 60 white colonies from each clone library was checked by vector-specific PCR with primers SP6 (5′-ATT TAG GTG ACA CTA TAG AAT AC-3′) and T7 (5′-TAA TAC GAC TCA CTA TAG GG-3′). Positive clones of each library were analyzed by DGGE at conditions described above, using bacterial primers 518f and 685r-GC, and eukaryotic primers NL1-GC and LS2. Profiles of individual clones were compared with each other and with the profile of the whole community. Clones with different profiles were sequenced using primers SP6 and T7 at a commercial facility (GATC-Biotech). The obtained sequences were compared with those present in the GenBank database using a BLAST search (http://blast.ncbi.nlm.nih.gov/Blast.cgi). The BLAST search generally was done using the "nucleotide collection" database, but several sequences, identified such as "uncultured bacterium" or "uncultured fungus," were also subjected to different BLAST searching using the bacterial and archaeal 16S rRNA database or excluding the uncultured/environmental sample sequences, respectively. The sequences were deposited in the GenBank database under the accession numbers KU363929–KU363956 (bacterial sequences) and KU363909–KU363928 (28S rRNA sequences).

Results

Fungal Micoflora Isolation and Detection

The culture-dependent strategy permitted the isolation of only few fungal strains; two members of the genus *Penicillium* (*Penicillium chrysogenum* and *Penicillium* sp.) were recovered from the photograph inv. 15438 and, from gelatin print inv. 27371F, *Alternaria* sp. and another *P. chrysogenum* were isolated.

The culture-independent approach showed divergences not only connected to the kind of nucleic acid analyzed (DNA or RNA) but also related to individual gelatine prints.

The eukaryotic microbiome of inv. 15438 was primarily characterized by the presence of *Malassezia restricta* and *Nectria haematococca* operational taxonomic units (OTUs), these fungi were detected by both DNA and RNA analysis. The DNA investigation permitted also the detection of *Malassezia globosa* and *Eurotium halophilicum*. The largest fungal diversity was detected through RNA analysis and was represented by *Cladosporium macrocarpum*, *Geotrichum* sp., *Saccharomyces cerevisiae*, and *Galactomyces candidum* (Fig. 1a, Table S1).

The eukaryotic community of inv. 27371F was detected mainly by the DNA strategy where several OTUs belong to *M. restricta*, uncultured compost fungus/*Geotrichum* sp., *G. candidum*, uncultured soil fungus clone/*Cladosporium ramotenellum*, *Cladosporium cladosporioides*, *Hyphodontia radula*, and *N. haematococca* were identified. The RNA-based approach showed only the presence of *M. restricta* (94% of detected clones) and of an acarus belonging to the genus *Demodex* (6%; Fig. 1b, Table S2).

Bacterial Assemblages

The bacterial community of inv. 15438 detected by DNA analysis was characterized by uncultured bacterium/*Streptococcus* spp. OTUs, which formed 62% of detected clones, followed by *Geobacillus* sp. with 29% and *E. coli* with 9%. By RNA were detected other kind of bacterial OTUs belonging to uncultured bacterium/*Acetobacterium bakii*, uncultured bacterium clone/*Staphylococcus epidermidis*, *Micrococcus* sp., *Enterobacter* sp., and *Bacillus cereus* (Fig. 1a, Table S3).

The bacterial DNA on gelatine inv. 27371F belonged mainly to the members of the order *Pseudomonadales* (*Acinetobacter*

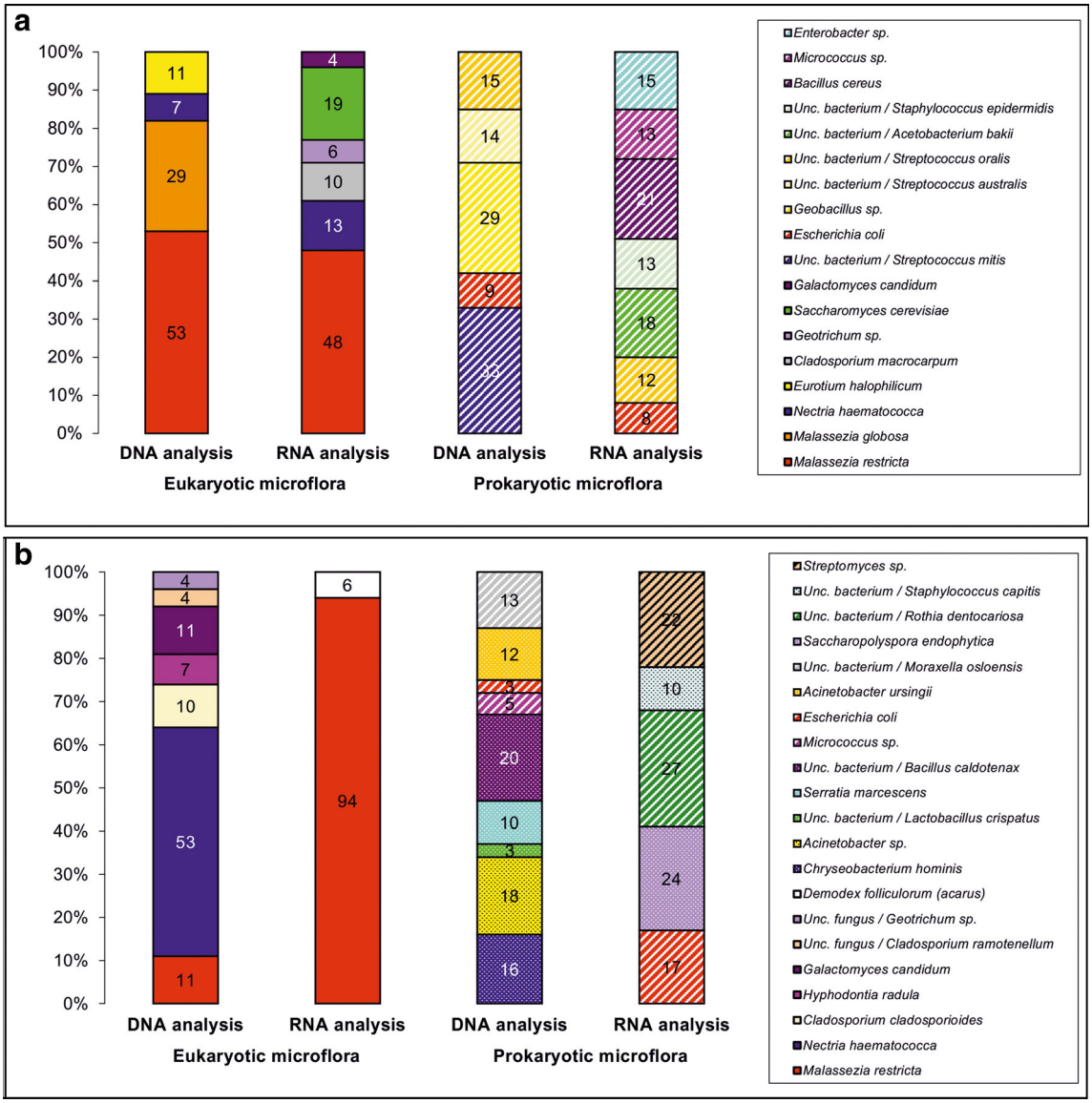

Fig. 1 Distribution of eukaryotic and bacterial communities on the surface of inv. 15438 (**a**) and inv. 27371F (**b**)

and uncultured bacterium/*Moraxella osloensis* OTUs) with 43% of detected clones. Other frequently detected OTUs included *Chryseobacterium hominis* and uncultured bacterium/*Bacillus caldotenax*, which reached the 16 and 20%, respectively. By RNA, the most representative bacterial group belonged to the Actinobacteria class (uncultured bacterium/*Rothia dentocariosa*, *Streptomyces* sp., and *Saccharopolyspora endophytica*) with 73% of OTUs. The analysis evidenced also the presence of *E. coli* and uncultured bacterium/*Staphylococcus capitis* (Fig. 1b, Table S4).

SEM-EDS Results

The samples collected directly from foxing-like stains on inv. 15438, examined by SEM, showed fungal features mainly referring to an *Aspergillus* species: large conidia single or in chain, slightly ovate, echinulate with prominent scars, and conidiophores with narrow vesicles finely covered with a layer of hairy structures (Fig. 2a, b). These features were very similar to those already observed in many other samples collected by the adhesive tape technique in previous surveys in other archives and libraries with similar mold contamination [22, 23]. Some fungal structures were attributed to *E. halophilicum* (An. *Aspergillus halophilicus*) (C.M. Chr., Papav. & C.R. Benj.) that could be identified also by light microscopy imaging (Fig. 2c). The structures appeared dried and collapsed. Some of the hyphae were thickened and covered by a material with a "waxy" appearance (Fig. 2a). Samples obtained from the stains affecting the print inv. 27371F showed biological material and filamentous masses that were not attributable to any defined species since no fruiting structures were actually documented.

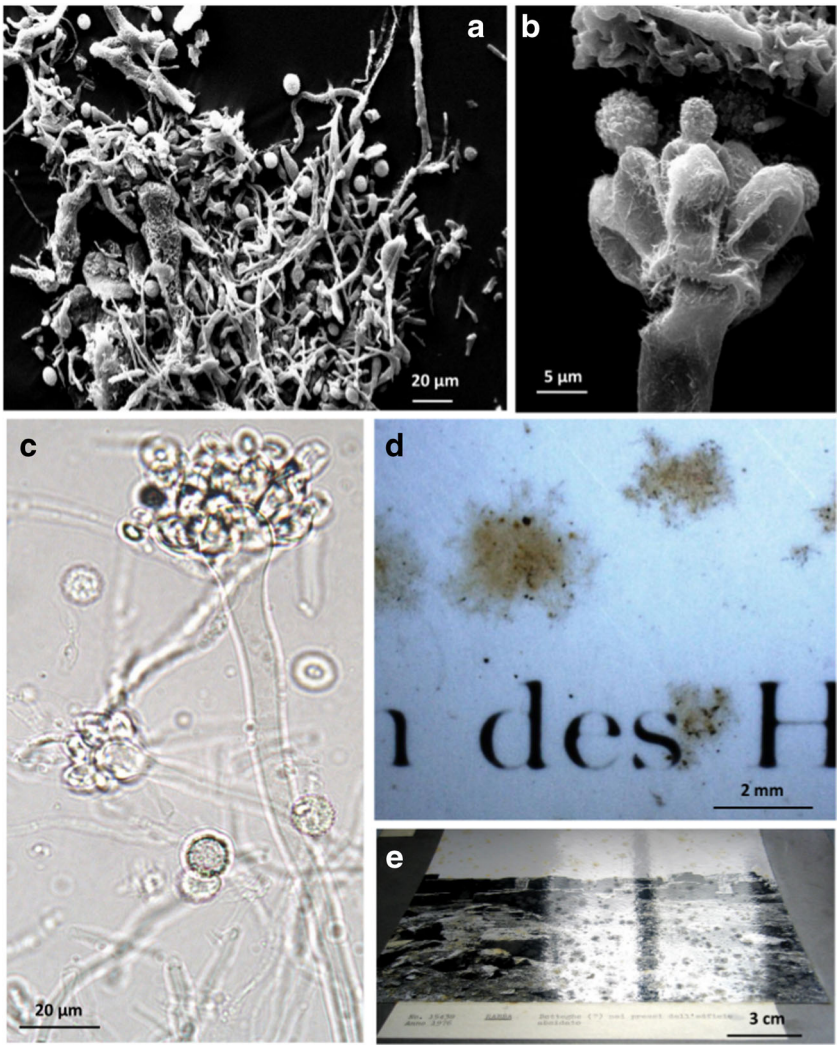

Fig. 2 **a** SEM image at HV, tungsten filament, 20 keV. Sample collected directly from foxing-like stains of inv. 15438, using the adhesive tape. The sample was sputtered with gold before observation. Fungal structures were attributed to *E. halophilicum* fungal species. **b** Detail of the fungal structures observed on inv. 15438. Image obtained on gold-sputtered sample with SEM-HV. **c** Adhesive tape sample bearing fungal structures sampled from inv. 15438 observed under light microscope, in bright field, with lactic acid preparation. **d** Detail of the foxing-like stains on gelatine. Image obtained with a stereomicroscope. **e** Inv. 15438 observed with raking light. The stains appeared rough and raised respect to the print's unaffected surface

The adhesive tape used in sampling collected, from both prints, some material that had spontaneously raised from the stains. The roughness and dusty appearance of the stains could be seen when observing the prints with stereomicroscope or raking light (Fig. 2d, e). The samples were observed by SEM–BSD imaging and analyzed by EDS (Fig. 3a–d, Tables 1, 2, and 3). Although the EDS results could not be considered quantitative, because of the unknown volumes scanned by the probe, the comparisons between elemental compositions of the samples, at any event analyzed according to identical modalities, yielded some statistically significant differences (Table 1). Namely, gelatine (or the surface) of the inv. 15438 contained more sulfur, while gelatine (or the surface) of the inv. 27371F contained more calcium. Both prints showed variable percentages, or traces, of inorganic compounds: Na, Mg, Al, Si, P, S, Ca, Ti, and Ba (Table 1). These elements were distributed with a different pattern between the components constituting the prints (Fig. 3). Ba was confined to the baryta layer only in samples obtained from the inv. 27371F (Table 2). The samples from inv. 15438 (Table 3) showed that, at least in the sampled stains, Ba was migrated also in gelatine. A sort of re-precipitation of Ba salts in gelatine was documented by SEM-BSD imaging (Fig. 3c) only in samples from the inv. 15438, with the formation of a mixture of organic amorphous material (presumably the same gelatine) mixed with particles, far below 1 µm, that appeared bright to the BSD detector. The gelatine samples obtained from the stains of inv. 27371F (Fig. 3b) appeared flaky and crossed by filamentous structures of possible biological origin. The elemental analysis of print's cross section from inv. 27371F (Fig. 3a) showed that the presence of Ti was associated mainly to the inner paper layer and, to a lesser extent, the baryta layer (Table 2).

RAMAN and XRF Results

XRF data showed the presence of Al, S, K, Ca, Ti, Fe, Br, Sr, and Ba in both the prints. The same elements, almost in the same concentration, were revealed also in the areas subjected to a biological attack.

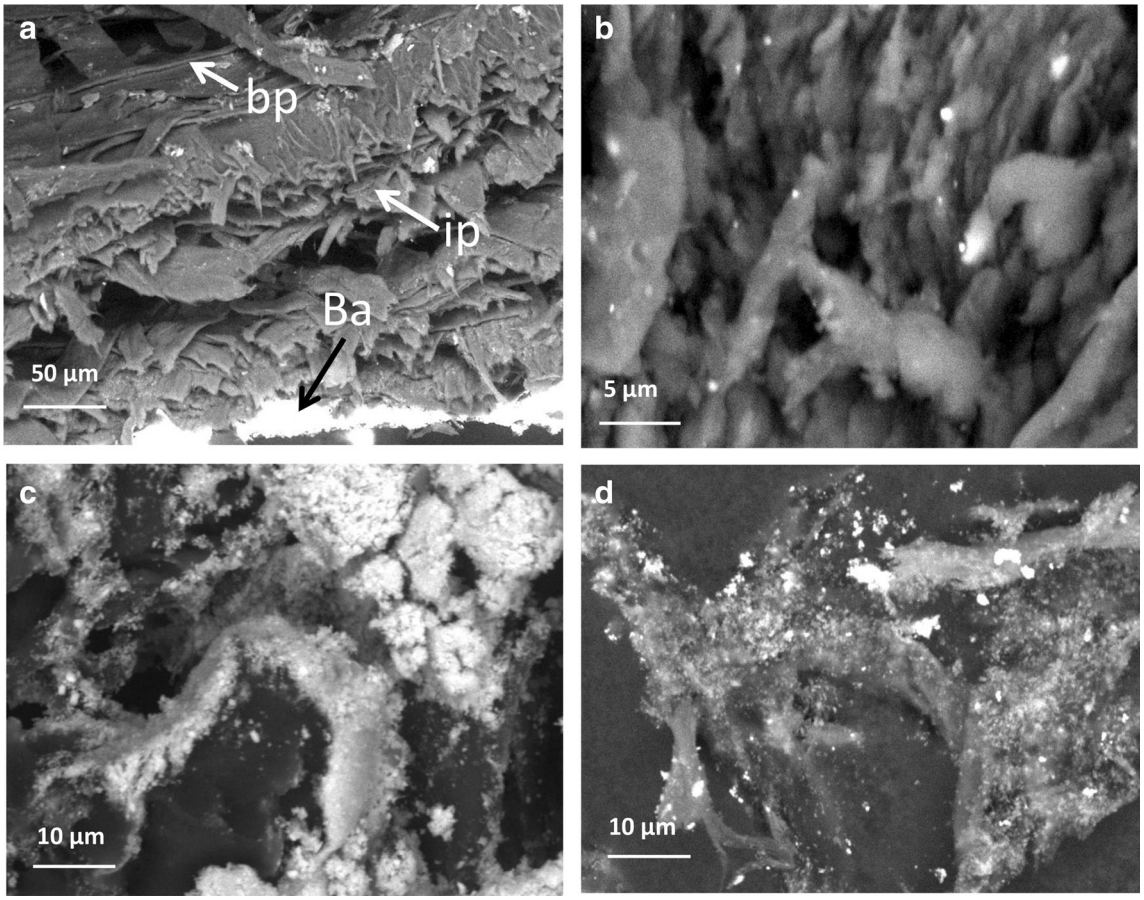

Fig. 3 SEM images obtained with BSD detector, tungsten filament, 20 keV. **a** Cross section of inv. 27371F. *bp* back paper, *ip* inner paper, *Ba* baryta layer. **b** Sample of gelatin layer from inv. 27371F. **c** Sample of gelatine layer mixed to baryta and other minerals from inv. 15438. **d** gelatine layer mixed with precipitated mineral nanoparticles from inv. 15438

Table 1 Comparison between average elemental composition (as weight %) of samples obtained from the stains of the two prints. Data were obtained from gelatine and barite samples taken from the spots with adhesive tape and analyzed by EDS after SEM observations. SEM images of the samples are shown in Fig. 3

	Inv. 15438 (n = 20)	Inv. 27371F (n = 25)
C	50.20 ± 2.38	53.4 0 ± 2.69
O	29.60 ± 1.40	33.50 ± 2.03
Na	0.01 ± 0.03	0.09 ± 0.03
Mg	0.09 ± 0.05	0.00 ± 0.00
Al	0.39 ± 0.13	1.07 ± 0.48
Si	0.22 ± 0.09	1.11 ± 0.50
P	0.04 ± 0.01^{b}	0.13 ± 0.02^{a}
S	3.36 ± 0.49^{a}	1.09 ± 0.38^{b}
Ca	0.03 ± 0.02^{b}	1.83 ± 0.59^{a}
Ti	1.46 ± 0.64	0.47 ± 0.21
Ba	14.50 ± 2.62	7.40 ± 3.25

Values are mean ± standard error of the mean. Means in a row without a common superscript letter differ ($P < 0.05$) as analyzed by one-way ANOVA and the Tukey's test

Before discussing the Raman results, it must be underlined that the co-occurrence of different species—both fungi and bacteria—on the photographic prints does not allow a detailed analysis of the spectra, since it is impossible to differentiate the contribution of each species.

Both examined prints were realized on baryta papers, with silver halide salts suspended in gelatine, as can be seen in Figs. 4 and 5, spectrum A, where the peaks at 453, 462, 618, 650, and 989 cm^{-1} are related to barium sulfate, whereas the signals in 1200–1750 cm^{-1} region are due to the contribution of gelatine: 1239 cm^{-1} amide III ß-sheet, 1550 cm^{-1} amide II ß-sheet, and 1650 cm^{-1} amide I α-helix. However, Raman spectroscopy showed a different interaction between microorganisms and the photographic support.

In the attacked areas of inv. 15438 (Fig. 4, spectrum B), the peaks at 438, 446, and 974 cm^{-1} are attributable to the formation of a phosphate, not yet exactly identified, but presumably a mixed aluminum-iron-potassium phosphate. All these elements were found by XRF analysis. The form of the peaks in the collected spectra lets us firstly hypothesize that the shift of the bands at lower wavenumbers could be attributed to the

Table 2 Comparison between average elemental composition (as weight %) of different areas spotted from the inv. 27371F. The data were obtained from gelatine and barite samples taken from the spots with adhesive tape and from 1-mm-thick samples of paper trimmed from the margins of the print. Samples were analyzed by EDS after SEM observations. SEM images of the samples are shown in Fig. 3 a, b

	Ba layer (n = 8)	Back paper (n = 9)	Gelatin (n = 12)	Inner paper (n = 8)
C	39.00 ± 6.40^{b}	45.00 ± 5.50^{b}	63.00 ± 2.10^{a}	51.00 ± 1.90^{ab}
O	19.00 ± 1.90^{c}	44.00 ± 2.90^{a}	32.00 ± 1.30^{b}	45.00 ± 0.99^{a}
Na	0.05 ± 0.05^{a}	0.01 ± 0.01^{a}	0.17 ± 0.04^{a}	0.03 ± 0.01^{a}
Al	0.24 ± 0.08^{b}	5.30 ± 2.00^{a}	0.18 ± 0.04^{b}	0.50 ± 0.08^{b}
Si	0.04 ± 0.03^{b}	5.50 ± 2.20^{a}	0.38 ± 0.11^{b}	0.22 ± 0.13^{b}
P	0.03 ± 0.03^{b}	0.00 ± 0.00^{b}	0.22 ± 0.03^{a}	0.00 ± 0.00^{b}
S	4.20 ± 1.10^{a}	0.09 ± 0.09^{b}	0.47 ± 0.05^{b}	0.04 ± 0.04^{b}
Ca	0.22 ± 0.06^{a}	0.00 ± 0.00^{a}	3.60 ± 1.00^{a}	0.29 ± 0.12^{a}
Ti	0.18 ± 0.18^{b}	0.09 ± 0.06^{b}	0.00 ± 0.00^{b}	2.30 ± 0.78^{a}
Ba	37.00 ± 6.60^{a}	0.00 ± 0.00^{b}	0.00 ± 0.00^{b}	0.00 ± 0.00^{b}

Values are mean ± standard error of the mean. Means in a row without a common superscript letter differ ($P < 0.05$) as analyzed by one-way ANOVA and the Tukey's test

differently hydrated barite, formed after interaction with microorganisms. No spectra of barites with different water content have been reported in the scientific literature. Therefore, we then decided to dissolve in water some samples of standard barite, let them re-precipitate, and performed analyses at different stages of hydration. No shifts were recorded with respect to the typical bands of standard barite. This evidence supported the assignment of the collected spectra to a phosphate. The 1200–1700 cm^{-1} region showed the formation of amorphous carbon, with peaks around 1351 and 1667 cm^{-1}.

Formation of a phosphate could be attributable to the activity of bacteria, like the *Bacillus* and *Streptomyces* species, that can produce alkaline phosphatase and hydrolyse phosphate monoester by enzymolysis in gelatine. PO_4^{3-} or HPO_4^{2-} could then react with metal cations [35]. The presence of phosphates in gelatine possibly derives from the manufacturing processes. Gelatine for photographic use is primarily alkaline-processed gelatine, especially for emulsion preparation. Photographic gelatine is generally made from ossein derived from bones, where the major salt is hydroxyapatite, a phosphate mineral. The leaching and transformation of phosphate forms by fungi and bacteria have been widely documented [17].

Barium was still present in the analyzed samples, as revealed by XRF, but in a different structure not detectable by Raman spectroscopy. Disappearance of barite could be attributable to the metabolic activity of microorganisms as it could have been absorbed and then differently re-precipitated, while the amorphous carbon can be interpreted as a byproduct of the consumption of gelatine by microorganisms.

The attacked areas of inv. 27371F (Fig. 5, spectrum B), instead, presented peaks at 234, 660, and 1055 cm^{-1} that can refer to the formation of a mixture of oxides, among them barium titanate. Also in this case, barium sulfate was no more detectable and it can be supposed that an interaction—different from that present in the inv. 15438—between microorganisms and barite took place, with a subsequent re-precipitation of barium in a configuration not detectable by Raman spectroscopy.

The ability of some fungi to promote extracellular biosynthesis of ternary oxide nanoparticles of barium titanate (BT) was described by Bansal et al. [6].

Also on this print, the 1200–1700 cm^{-1} region of the spectrum showed the formation of amorphous carbon, with peaks around 1351 and 1667 cm^{-1}.

Table 3 Comparison between average elemental composition (as weight %) of different areas spotted from the inv. 15438. The data were obtained from gelatine and barite samples taken from the spots with adhesive tape. Samples were analyzed by EDS after SEM observations. SEM images of the samples are shown in Fig. 3c, d

	Ba layer (n = 9)	Gelatine (n = 7)	Paper fibers (n = 7)
C	44.00 ± 4.00^{b}	57.00 ± 2.30^{a}	52.00 ± 2.20^{ab}
O	31.00 ± 2.20	27.00 ± 2.60	31.00 ± 1.70
Na	0.00 ± 0.00 ^{b}	0.28 ± 0.05^{a}	0.00 ± 0.00^{b}
Mg	0.00 ± 0.00 ^{b}	0.00 ± 0.00^{b}	0.46 ± 0.17^{a}
Al	0.00 ± 0.00 ^{b}	0.97 ± 0.24^{a}	0.24 ± 0.03^{b}
Si	0.08 ± 0.04^{b}	0.06 ± 0.04^{b}	0.80 ± 0.29^{a}
P	0.03 ± 0.01^{b}	0.00 ± 0.00^{b}	0.12 ± 0.04^{a}
S	4.50 ± 0.84	2.10 ± 0.61	2.90 ± 0.57
Ca	0.02 ± 0.02^{b}	0.00 ± 0.00^{b}	0.12 ± 0.04^{a}
Ti	0.20 ± 0.10^{b}	3.60 ± 1.60^{a}	0.45 ± 0.05^{ab}
Ba	20.00 ± 4.00	8.50 ± 4.30	12.00 ± 2.70

Values are mean ± standard error of the mean. Means in a row without a common superscript letter differ ($P < 0.05$) as analyzed by one-way ANOVA and the Tukey's test

Discussion

The microbial community present on foxing stains of two gelatin photographs was assessed by cultivation and culture-independent strategies. The latter approach was based on both DNA and RNA analyses. The DNA investigation

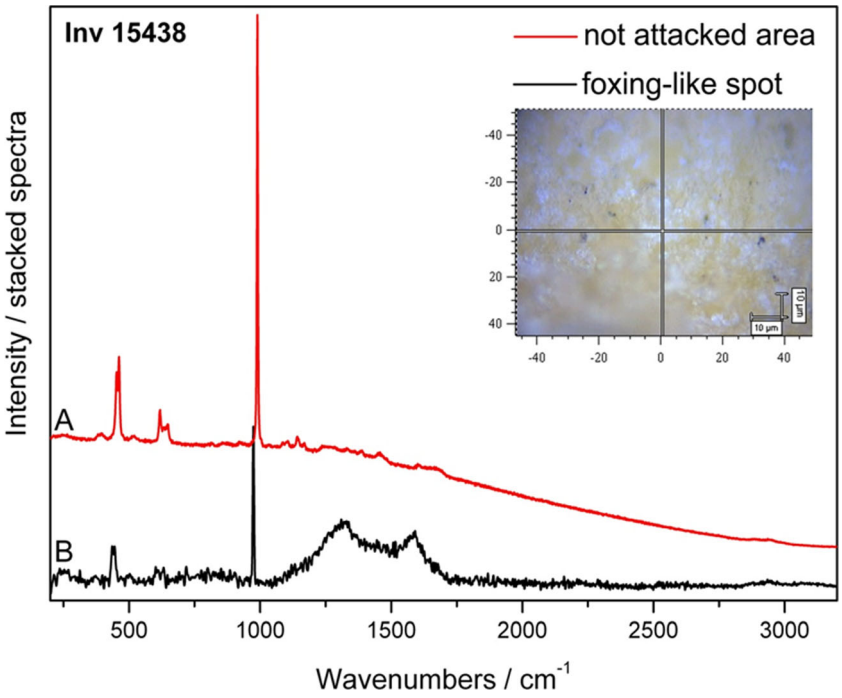

Fig. 4 Raman spectra collected from the photograph inv. 15438. *A* area not attacked by microorganism; barium sulfate and gelatine are well visible. *B* foxing-like spot (image in the *inset*) with formation of phosphates and amorphous carbon

showed which species of microorganisms were able to colonize this multilayer material during the time, and the RNA investigation gave a picture of the living microbiome actually colonizing the photograph surfaces at the time of the sampling. It was noted that a high degree of complementarity exists between DNA and RNA results. Only few microbial species were identified by both of these analytical approaches. Moreover, little overlap between the lists of species obtained from the two prints was observed. The microbiome detected both by DNA and RNA sequencing approaches from the print inv. 15438 included the OTUs of *M. restricta* and *N. haematococca* for fungi and uncultured bacterium/ *Streptococcus oralis* and *E. coli* for bacteria. Among these, only *M. restricta* and *E. coli* were detected also on the gelatin print 27371F.

N. haematococca is mainly a plant pathogen and is the teleomorph of *Fusarium solani*. The fungi of this genus occurred frequently in archival environments [7, 24, 29] and

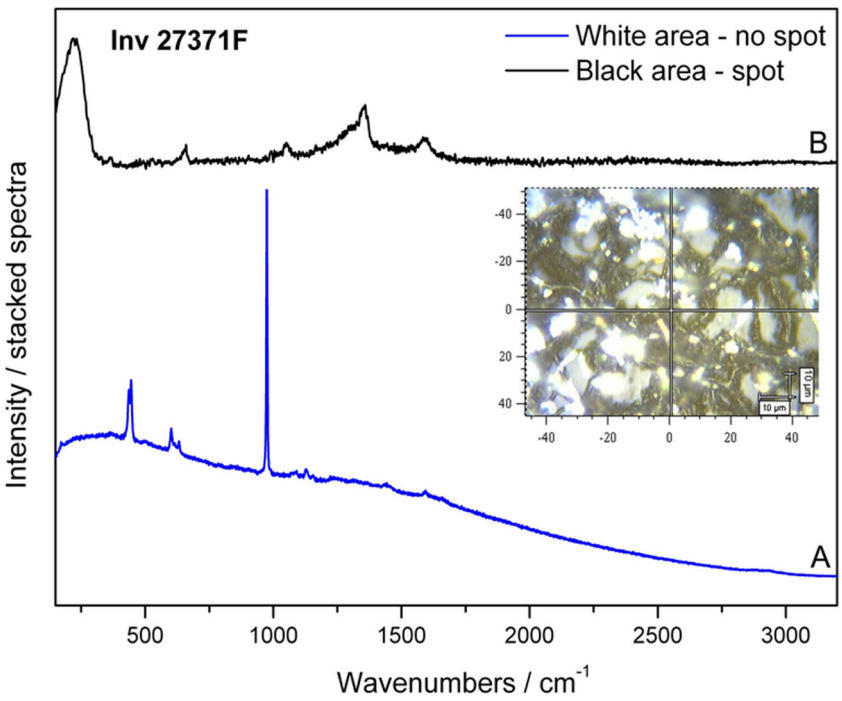

Fig. 5 Raman spectra collected from the photograph inv. 27371F. *A* area not attacked by microorganism; barium sulfate and gelatine are well visible. *B* black area subjected to a biological attack (image in the *inset*) with formation of mixed oxides and amorphous carbon

their lignocellulolytic activity is already known. Therefore, the presence of living *F. solani* indicates a potential risk of biodeterioration of these gelatin prints. The members of the genus *Malassezia* are more associated with human contamination; in fact, they normally colonize the epidermis [15]. Such kinds of fungi were identified by both culture-independent approaches and in both photographs. Unfortunately, the knowledge about the hydrolytic properties of this kind of fungal genus is limited. DNA analysis showed the presence on inv. 15438 of another typical colonizer of archive and library documents, *E. halophilicum* [22]. Its living state was not confirmed by RNA identification, but its presence in foxing stains was profusely documented by SEM imaging. It is like that such fungus acted as a pioneer and colonized the print surface spreading during a single event that took place in the past; following its death, different fungal biodeteriogens, such as members of *Galactomyces*/*Geotrichum* group, *Cladosporium*, and *Saccharomyces*, took over its place on gelatin print inv. 15438.

On inv. 27371F print, it seems that the most dangerous fungal deteriogens occurred at the early phase of contamination; fungi such as *N. haematococca*, *H. radula*, *Galactomyces*/*Geotrichum*, and *Cladosporium* members were detected exclusively by DNA. *M. restricta* and the acarus *Demodex folliculorum*, revealed by RNA cloning, were the only living organisms on photograph surface.

The DNA-based analysis of the bacterial community on inv. 15438 revealed a series of uncultured bacteria/*Streptococcus* spp. typical of human origin. Indeed, the species *S. mitis*, *S. oralis*, and *S. australis* are considered as normal microorganisms of the oral cavity [1].

The number of species associated to man and found alive on these materials (fungi, acari, and bacteria) suggested that a massive source of contamination of photographic materials was human manipulation.

Living bacteria at the time of sampling (those detected using RNA sequencing) were *B. cereus*, *Micrococcus* sp., and *Enterobacter* sp., which often contaminate the archival items and possess marked hydrolytic abilities [8, 16, 18, 33].

A different bacterial microbiome was identified on the surface of inv. 27371F, where the differences between the past and recent contaminations were more marked. The microbiome detected by RNA analysis (recent contamination) was composed mainly by actinobacteria belonging to the genera *Rothia*, *Streptomyces*, and *Saccharopolyspora*. These kinds of bacteria were already detected in museum environments and some of them can be considered as halotolerant strains [27] with cellulolytic and proteolytic properties [10, 25, 28]. The DNA sequencing was able to detect a larger and different diversity compared to RNA analysis. By DNA analysis, only one member (*Micrococcus* sp.) representing the phylum *Actinobacteria* was detected, while the phylum *Proteobacteria* was predominant, followed by the phyla *Firmicutes* and *Bacteroidetes*. Except of *C. hominis*, all the other bacterial genera (*Acinetobacter*, *Bacillus*, *Lactobacillus*, and *Micrococcus*), including members of the order *Enterobacteiales*, were previously detected on items or archival and library environments [2, 7, 8, 16, 30].

It is possible to summarize that on both prints, in correspondence of the foxing-like stains, a biofilm was detected, which mainly consisted of halotolerant fungal and bacterial species that settled over the cellular material of some other microbial species starving or dead, and a few living microorganisms, possibly deriving from a more recent manipulation. The presence of potentially halotolerant species could be due to the content of various salt complexes within the gelatine prints, including those that microorganisms can deposit during colonization.

SEM-EDS, μ-RAMAN, and XRF succeeded in distinguishing the manufacture of the two prints and the structural changes occurring in the attacked areas in contrast to those not attacked. In particular, the differences in the composition of the two prints (i.e., the presence of Ti in paper, the concentration of Ca) could account for a different attack by fungal and bacterial species, followed by the development of distinct communities on the two objects. Differences in elemental composition between the prints and the relevant layers obtained using EDS were based on repeated measurements obtained from a number of small samples gained from the materials and mounted in the SEM chamber, while XRF data were obtained from several areas selected on the entire prints. A few differences between the results obtained with the two different techniques could account for the different kinds of measured objects (samples taken from prints and the prints themselves). In particular, in the print inv. 15438, XRF analyses detected Al in the baryta layer, while EDS failed to identify the Al peak.

The activity of fungal and bacterial members growing on the prints resulted also in a modification of the mineral components present in the materials' layers. In the attacked areas of inv. 15438, formation of a phosphate was documented, presumably a mixed aluminum-iron-potassium phosphate that could be attributed to the hydrolytic activity of bacteria. Also the disappearance of barite in the attacked areas could be attributed to the metabolic activity of microorganisms: barite could have been leached and differently re-precipitated in a configuration not detectable by Raman spectroscopy. The attacked areas of inv. 27371F showed the formation of a mixture of oxides and also a change in the barium sulfate chemical forms. Again, the ability of some fungi to promote the extracellular biosynthesis of ternary oxides could have had a role in the observed phenomena.

Although the two prints displayed differences in microbial species and chemical composition, the common denominator of the identical foxing-like stains could be searched in the aging of the biological biofilm settled on their surface.

According to Arai [4], biological foxing stains on paper are formed due to the presence of glucose and amino acids. The

author showed that fungal metabolic excretions, particularly aminobutyric acid, alanine, glycine, ornithine, and serine, can lead to the staining of paper in a foxing-type pattern. These organic chemicals, if mixed and applied in drops on paper, and then kept for 40 days at a_w 0.75 and 0.84 and 20–35 °C, reacted together and resulted in the appearance of brown spots. Hence, Arai [4] considered that foxing caused by fungi is the result of a browning chemical reaction (Maillard reaction) that takes place between cello-oligosaccharides and aminobutyric acid and other amino acids, which are produced by growing absolute tonophilic fungi on paper [3]. At the same time, Florian and Manning [14] studied the role of fungi in foxing by light and electron microscopy. They found that, in some cases, the initial cause of foxing was actually a group of spores of conidia that had been deposited on the surface of paper prior to printing and had germinated in situ during the slow drying of the paper.

The presence of dead fungal and bacterial debris, settled in a series of contamination events to which the photographic prints had been exposed in the past, was actually the common denominator of the damage affecting the two objects.

Conclusions

The study distinguished the manufacture of the two prints, using SEM-EDS and XRF, and described the structural and chemical changes occurring in attacked areas in contrast to those not attacked, using μ-RAMAN. To the best of our knowledge, researches that could combine such a chemical investigation with molecular and microbiological study of photographic materials, using non-destructive methods, has not been published before. The outcomes showed that the differences in the composition of the two prints accounted for a different attack by fungal and bacterial species, investigated by DNA- and RNA-based approaches, which displayed the development of distinct communities. Moreover, a close interaction between the microorganisms and the minerals (barium, sulfates, phosphates, etc.) was documented in the damaged areas. The mechanism proposed could be summarized in this way: the production of the stains depended from the settlement and growth of halotolerant fungi and bacteria that produced localized "hot spots" of organic material on gelatin. These compounds, which comprised sugars and proteins, induced during aging a browning chemical reaction that stained gelatin and modified also the local mineral chemistry. The presence of dead fungi remaining on the photographic prints still represents a reason of concern since their contents of potentially reactive chemicals is as menacing as the living fungi themselves, from a conservation point of view.

This investigation evidenced that bacterial and fungal interactions with mineral components and organic compounds, of which photographic materials are made, could lead to complex and quite different staining and spoiling mechanisms that are worthy of being further analyzed and understood. It is of basic and extreme importance for this sector to carry out research based on simulation of the interaction of fungi and bacteria with compounds like barite and gelatine in model samples and in particular to establish a causative relationship between halotolerant species and the formation of foxing stains on gelatine prints.

Acknowledgements This work was financed by the Slovak VEGA Agency, project number: 2/0103/14 "Protecting our memories: investigation into the biodeterioration of photographic and cinematographic materials."

We would like also to acknowledge Dr. Lavinia Ciuffa Acting Curator of the Photographic Archive of American Academy in Rome for her availability and for proving us the opportunity to study these interesting prints.

References

1. Aas JA, Paster BJ, Stokes LN, Olsen I, Dewhirst FE (2005) Defining the normal bacterial flora of the oral cavity. J. Clin. Microbiol. 43:5721–5732
2. Abrusci C, Marquina D, Del Amo A, Catalina F (2007) Biodegradation of cinematographic gelatin emulsion by bacteria and filamentous fungi using indirect impedance technique. Int Biodeterior Biodegradation 60:137–143
3. Arai H (1987) Microbiological studies on the conservation of paper and related cultural properties. Part 5: physiological and morphological characteristics of fungi isolated from foxing, formation mechanisms and countermeasures. Sci Conserv 26:43–52
4. Arai H (2000) Foxing caused by fungi: twenty-five years of study. Int Biodeterior Biodegradation 46:181–188
5. Ardizzone E, Dindo H, Mazzola G (2008) A set of low-level descriptors for images affected by foxing. In Proc. of the 16th European Signal Processing Conference (EUSIPCO). http://www.eurasip.org/Proceedings/Eusipco/Eusipco2008/
6. Bansal V, Poddar P, Ahmad A, Sastry M (2006) Room-temperature biosynthesis of ferroelectric barium titanate nanoparticles. J. Am. Chem. Soc. 128:11958–11963
7. Borrego S, Lavin P, Perdomo I, Gómez de Saravia S, Guiamet P (2012) Determination of indoor air quality in archives and biodeterioration of the documentary heritage. ISRN Microbiol Article ID 680598, doi: 10.5402/2012/680598.
8. Borrego S, Guiamet P, de Saravia SG, Batistini P, Garcia M, Lavin P, Perdomo I (2010) The quality of air at archives and the biodeterioration of photographs. Int Biodeterior Biodegradation 64:139–145
9. Buchholz-Cleven BE, Rattunde B, Straub KL (1997) Screening for genetic diversity of isolates of anaerobic Fe (II)-oxidizing bacteria using DGGE and whole-cell hybridization. Syst. Appl. Microbiol. 20:301–309
10. Bučková M, Puškárová A, Sclocchi MC, Bicchieri M, Colaizzi P, Pinzari F, Pangallo D (2014) Co-occurrence of bacteria and fungi and spatial partitioning during photographic materials biodeterioration. Polym. Degrad. Stab. 108:1–11
11. Cocolin L, Aggio D, Manzano M, Cantoni C, Comi G (2002) An application of PCR-DGGE analysis to profile the yeast populations in raw milk. Int. Dairy J. 12:407–411
12. Coluzza C, Bicchieri M, Monti M, Piantanida G, Sodo A (2008) Atomic force microscopy application for degradation diagnostics in library heritage. Surf. Interface Anal. 40:1248–1253

13. Dusan S, Kaplan A (2013) The atlas of analytical signatures of photographic processes. Los Angeles, CA: Getty Conservation Institute. http://hdl.handle.net/10020/gci_pubs/atlas_analytical
14. Florian MLE, Manning L (2000) SEM analysis of irregular fungal spot in an 1854 book: population dynamics and species identification. Int Biodeterior Biodegradation 46:205–220
15. Gupta AK, Batra R, Bluhm R, Boekhout T, Dawson TL (2004) Skin diseases associated with *Malassezia* species. J. Am. Acad. Dermatol. 51:785–798
16. Karbowska-Berent J, Górny RL, Strzelczyk AB, Wlazło A (2011) Airborne and dust borne microorganisms in selected Polish libraries and archives. Build. Environ. 46:1872–1879
17. Kucey RMN (1983) Phosphate solubilizing bacteria and fungi in various cultivated and virgin Alberta soils. Can. J. Soil Sci. 63:671–678
18. Kraková L, Chovanová K, Selim SA, Šimonovičová A, Puškarová A, Maková A, Pangallo D (2012) A multiphasic approach for investigation of the microbial diversity and its biodegradative abilities in historical paper and parchment documents. Int Biodeterior Biodegradation 70:117–125
19. Kurtzman CP, Robnett CJ (1998) Identification and phylogeny of ascomycetous yeasts from analysis of nuclear large subunit (26S) ribosomal DNA partial sequences. Antonie Van Leeuwenhoek 73:331–371
20. Lane DJ (1991) 16S/23S rRNA sequencing. In: Stackenbrandt E, Goodfellow M (eds) Nucleic acid techniques in bacterial systematics. John Wiley and Sons, New York, pp. 115–148
21. Lourenço MJ, Sampaio JP (2009) Microbial deterioration of gelatin emulsion photographs: differences of susceptibility between black and white and colour materials. Int Biodeterior Biodegradation 63:496–502
22. Micheluz A, Manente S, Tigini V, Prigione V, Pinzari F, Ravagnan G, Varese GC (2015) The extreme environment of a library: xerophilic fungi inhabiting indoor niches. Int Biodeterior Biodegradation 99:1–7
23. Montanari M, Melloni V, Pinzari F, Innocenti G (2012) Fungal biodeterioration of historical library materials stored in Compactus movable shelves. Int Biodeterior Biodegradation 75:83–88
24. Nunes I, Mesquita N, Verde SC, Bandeira AML, Carolino MM, Portugal A, Botelho ML (2013) Characterization of an airborne microbial community: a case study in the archive of the University of Coimbra, Portugal. Int Biodeterior Biodegradation 79:36–41
25. Pangallo D, Kraková L, Chovanová K, Bučková M, Puškarová A, Šimonovičová A (2013) Disclosing a crypt: microbial diversity and degradation activity of the microflora isolated from funeral clothes of Cardinal Peter Pázmány. Microbiol. Res. 168:289–299
26. Piantanida G, Pinzari F, Montanari M, Bicchieri M, Coluzza C (2006) Atomic force microscopy applied to the study of Whatman paper surface deteriorated by cellulolytic filamentous fungus. Macromol. Symp. 238:92–97
27. Piñar G, Sterflinger K, Pinzari F (2015) Unmasking the measles-like parchment discoloration: molecular and microanalytical approach. Environ. Microbiol. 17:427–443
28. Puškárová A, Bučková M, Habalová B, Kraková L, Maková A, Pangallo D (2016) Microbial communities affecting albumen photography heritage: a methodological survey. Sci Rep 6:20810
29. Rakotonirainy MS, Arnold S (2008) Development of a new procedure based on the energy charge measurement using ATP bioluminescence assay for the detection of living mould from graphic documents. Luminescence 23:182–186
30. Skóra J, Gutarowska B, Pielech-Przybylska K, Stępień Ł, Pietrzak K, Piotrowska M, Pietrowski P (2015) Assessment of microbiological contamination in the work environments of museums, archives and libraries. Aerobiologia 31:389–401
31. Sneath PH, Sokal RR (1973) Numerical taxonomy. The principles and practices of numerical classification. WF Freeman and Co, San Francisco
32. Stanco F, Tenze L, Ramponi G (2005) Virtual restoration of vintage photographic prints affected by foxing and water blotches. J Electron Imaging 14:043008
33. Troiano F, Polo A, Villa F, Cappitelli F (2014) Assessing the microbiological risk to stored sixteenth century parchment manuscripts: a holistic approach based on molecular and environmental studies. Biofouling 30:299–311
34. White TJ, Bruns T, Lee S, Taylor J (1990) Amplification and direct sequencing of fungal ribosomal RNA genes for phylogenetics. In: Innis MA, Gelfand DH, Sninsky JJ, White TJ (eds) PCR protocols: a guide to methods and applications. Academic Press, London, pp. 315–321
35. Yu X, Qian C, Wang X (2016) Morphology of barium hydrogen phosphate formation induced by phosphate-mineralization microbe. J Wuhan Univ Technol Mater Sci Ed 31:227–230